Dynamics of Bose-Einstein recondensation in higher bands

Vaibhav Sharma [1,*] Sayan Choudhury,[2,†] and Erich J. Mueller [1,‡]
[1]*Laboratory of Atomic and Solid State Physics, Cornell University, Ithaca, New York 14853, USA*
[2]*Department of Physics and Astronomy, University of Pittsburgh, Pittsburgh, Pennsylvania 15260, USA*

(Received 12 November 2019; accepted 20 February 2020; published 12 March 2020)

Motivated by recent experiments, we explore the kinetics of Bose-Einstein condensation in the upper band of a double-well optical lattice. These experiments engineer a nonequilibrium situation in which the highest energy state in the band is macroscopically occupied. The system subsequently relaxes and the condensate moves to the lowest energy state. We model this process, finding that the kinetics occurs in three phases: The condensate first evaporates, forming a highly nonequilibrium gas with no phase coherence; energy is then redistributed among the noncondensed atoms; finally, the atoms recondense. We calculate the timescales for each of these phases and explain how this scenario can be verified through future experiments.

DOI: 10.1103/PhysRevA.101.033609

I. INTRODUCTION

The kinetics of ordering is one of the iconic problems in physics, with relevance to areas as diverse as cosmology and metallurgy [1–6]. New tools have evolved in cold atom systems which enable the controlled study of ordering, and which are yielding unconventional ordering scenarios [7–10]. Recent experiments at MIT [11,12] and Hamburg [13–15] have observed nonequilibrium Bose-Einstein condensation in the first excited band of a bipartite optical lattice. Similar physics is seen in Floquet lattices [16–19]. Motivated by these experiments, we study the dynamics of bosons which are condensed in the highest energy state of the first excited band of a double-well optical lattice. The system subsequently evolves to a Bose-Einstein condensate (BEC) in the lowest energy state of that band. We model this process, finding that the condensate first evaporates, then recondenses. This paradigm is very different from those traditionally used to model order parameter dynamics, and should have broad impact on understanding other nonequilibrium systems.

Beyond their intrinsic intellectual merit, these nonequilibrium experiments are motivated by attempts to produce exotic states of matter. The final state in the MIT experiment displays a supersolid stripe phase [11,12]. Other higher band geometries produce even more exotic physics, ranging from multiflavor and multiorbital Hubbard models [13–15,20–25] to the formation of interaction-induced chiral order related to p-wave superconductivity [26,27] or chiral Bose liquids [28]. A recent experiment has demonstrated the presence of a dynamical sliding phase, when P-band bosons are loaded in an one-dimensional optical lattice [29]. One needs at least a qualitative understanding of the higher-band kinetics before one can reliably design protocols for producing these states.

The model we use for analyzing the higher band kinetics can also be applied in other settings, including the simpler case of a Bose-Einstein condensate in the lowest band of an optical lattice. In that case, the analogous stating point would be when all of the atoms are condensed in the highest energy state of the band. This could be arranged by using Raman lasers, or an external force. Alternatively, as shown in Ref. [30], one can "shake" the lattice to induce an inverted floquet band structure. To keep our narrative as simple as possible, we will focus on the upper-band case, which motivated our study. Limited discussion of timescales in these other experiments is given in Sec. VIII. Some related theoretical work has also been done by Garcia *et al.* [31] for a different model where they study the coherent dynamics and fragmentation of a BEC in a single double well potential with three modes that is quenched to a superposition state of ground and first excited mode.

Our paper is organized as follows. In Sec. II, we introduce a model for analyzing the dynamics of a BEC loaded in a double well optical lattice. In Sec. III, we use thermal equilibrium arguments to determine the properties of the system for $\tau_N \ll t \ll \tau_{ab}$, where τ_N is the microscopic scattering time in the higher band and τ_{ab} is the time for decay from the upper to lower band. In Secs. IV and V, we describe the kinetics of condensation in the excited band, calculating τ_N and exploring the other timescales in the dynamics. In Sec. VI, we calculate τ_{ab} and verify that $\tau_{ab} \gg \tau_N$, guaranteeing that one can produce a metastable condensate in the excited band. In Sec. VII, we discuss how time-of-flight images can be used to observe the dynamics of higher band bosons and finally in Sec. VIII, we discuss how our model may be applied to experimental settings beyond higher bands, such as inverted bands.

II. MODEL

A. Single-particle Hamiltonian

Motivated by the MIT experiment [11,12], and related experiments at Hamburg [13–15], we model the dynamics of

*vs492@cornell.edu
†sc2385@cornell.edu
‡em256@cornell.edu

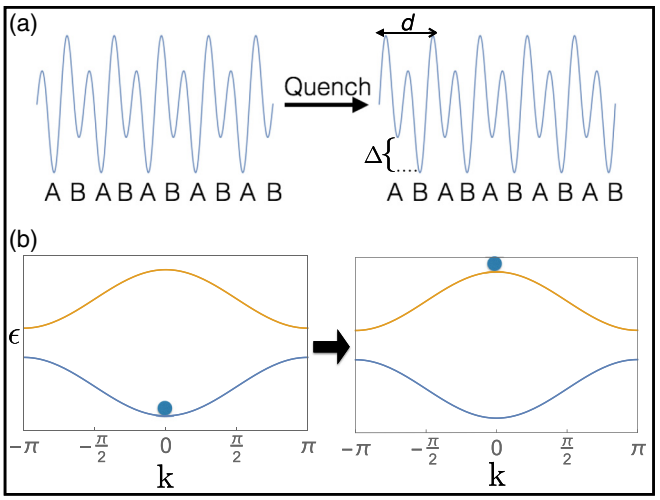

FIG. 1. (a) Envisioned setup for the experiment. (b) Visualizing how the condensate gets transferred from the lower band to the highest energy state in the upper band after quench

a BEC loaded into a double-well optical lattice. A schematic of the setup is shown in Fig. 1(a). The single-particle Hamiltonian, H_0 describing this system is given by

$$H_0 = \int d^2\mathbf{r}_\perp \sum_i \Delta(t)\, b_i^\dagger b_i - (J_1 a_i^\dagger b_i + J_2 a_i^\dagger b_{i-1} + \text{H.c.}) + \frac{\hbar^2}{2m}(\boldsymbol{\nabla}_\perp b_i^\dagger \boldsymbol{\nabla}_\perp b_i + \boldsymbol{\nabla}_\perp a_i^\dagger \boldsymbol{\nabla}_\perp a_i), \tag{1}$$

where the lattice is in the z direction. The transverse spatial components are suppressed: $a_i = a_i(\mathbf{r}_\perp)$ is the annihilation operator for a boson at site i of the A sublattice where $r_\perp = (x, y)$ and $\boldsymbol{\nabla}_\perp = \hat{x}\partial_x + \hat{y}\partial_y$. The operators b_j have analogous meaning for the B sublattice. For this paper, we consider the case $J_1 = J_2 = J'$.

Before the start of the experiments, the energy offset between the A and B sites, $\Delta(t < 0) = \Delta$ and the BEC is in the state $\mathbf{k} = \mathbf{0}$ of the lowest band. The experimental protocol then involves changing the lattice depths very fast such that after the quench, $\Delta(t > 0) = -\Delta$.

The single-particle Hamiltonian is diagonal in momentum space as shown in Appendix A, and the dispersion for the higher band is

$$\epsilon_\mathbf{k} = J[1 + \cos(k_z d)] + \frac{\hbar^2 k_\perp^2}{2m}, \tag{2}$$

where $J = 2(J')^2/\Delta$, and d is the length of the unit cell. Here $\mathbf{k}_\perp$ can be arbitrary, but $-\pi/d < k_z < \pi/d$. The band eigenstates are also derived in Appendix A.

The $k = 0$ state in the lowest band before the quench has nearly unit overlap with the post-quench $k = 0$ state in the upper band, and the quench projects the condensate into the higher band. A similar approach has been used to create an excited band BEC in a two-dimensional checkerboard lattice [13–15].

As we argue below, the timescale for atoms to equilibrate in the upper band is much smaller than band-relaxation. Thus, we predominantly study single-band kinetics, using the dispersion in Eq. (2).

B. Interactions

The kinetics are driven by point interactions,

$$H_{\text{int}} = \frac{g}{2}\int d^3r\, \psi^\dagger(r)\psi^\dagger(r)\psi(r)\psi(r), \tag{3}$$

where $g = 4\pi\hbar^2 a_s/m$, with scattering length a_s. The field operators, projected into our single band, are expressed as

$$\psi(\mathbf{r}) = \sum_j \bar{a}_j(\mathbf{r}_\perp) w(z - z_j), \tag{4}$$

where $w(z)$ is the Wannier state and $z_j = jd$ is the location of the jth site. Neglecting the overlap between Wannier states on distinct sites, one arrives at an effective δ-function interaction in each plane, which can be written as either an integral or a sum in momentum space:

$$H_{\text{int}} = \frac{U}{2}\frac{V^2 d}{(2\pi)^9}\int d^3k_1 d^3k_2 d^3k_3\; \bar{a}^\dagger_{\mathbf{k}_1}\bar{a}^\dagger_{\mathbf{k}_2}\bar{a}_{\mathbf{k}_3}\bar{a}_{\mathbf{k}_1+\mathbf{k}_2-\mathbf{k}_3} \sim \frac{U}{2}\frac{d}{V}\sum_{k_1k_2k_3}\bar{a}^\dagger_{\mathbf{k}_1+\mathbf{k}_2-\mathbf{k}_3}\bar{a}^\dagger_{\mathbf{k}_3}\bar{a}_{\mathbf{k}_2}\bar{a}_{\mathbf{k}_1} \tag{5}$$

In the second form, the sum is over $k = 2\pi n/L$ and $V = L^3$, where L is a multiple of d. The operator $a_\mathbf{k}$ is defined in Eq. (A1). In either case,

$$U = \frac{4\pi\hbar^2 a_s}{m}\int dz |w(z)|^4 = \frac{4\pi\hbar^2 a_s}{m d_a}.$$

The last equality defines the characteristic width of the Wannier state d_a. Note, that in contrast to the standard Hubbard U, which is an energy, here U has units of energy times length squared. This structure occurs because the atoms are free to move perpendicular to the lattice.

III. STEADY STATE

The long-time behavior in the upper band is solely determined by conservation laws. After the quench, the kinetic energy is $E = 2NJ$. In the absence of band relaxation, the system will evolve so that there are N_π atoms in the condensate at $\mathbf{k_c} = (k_x = k_y = 0, k_z = \pi/d)$ and N_{nc} noncondensed atoms. According to the higher band dispersion, only the noncondensed atoms contribute to the kinetic energy. Neglecting interactions, their number and kinetic energy are

$$\frac{N_{\text{nc}}}{V} = \int\frac{d^3k}{(2\pi)^3} f_k = \frac{\rho_0 J}{4\pi^2}F(\beta J) = \int d\epsilon\, \rho(\epsilon) f(\epsilon),$$
$$\frac{E_{\text{nc}}}{V} = \int\frac{d^3k}{(2\pi)^3}\epsilon_\mathbf{k} f_k = \frac{\rho_0 J^2}{4\pi^2}G(\beta J) = \int d\epsilon\, \epsilon\rho(\epsilon) f(\epsilon), \tag{6}$$

where the density of states is

$$\tilde{\rho}(\epsilon) = \frac{\rho(\epsilon)}{\rho_0} = \begin{cases} 1 & \epsilon \geqslant 2J, \\ \frac{1}{\pi}\cos^{-1}\left(1 - \frac{\epsilon}{J}\right) & \epsilon < 2J, \end{cases} \tag{7}$$

with $\rho_0 = m/\hbar^2 d$. The characteristic length of the system is $(\rho_0 J)^{-1/3}$.

Equations (6) define the dimensionless functions F and G. The Bose occupation factors are $f_k = f(\epsilon_{\mathbf{k}}) = [\exp(\beta\epsilon_{\mathbf{k}}) - 1]^{-1}$, in which we have taken the chemical potential to vanish, corresponding to the conditions for having a condensate at $\mathbf{k_c}$. The density of states is three-dimensional at small ϵ, $\rho(\epsilon \to 0) \sim \sqrt{\epsilon}$, and two-dimensional at large ϵ, $\rho(\epsilon \to \infty) \sim \epsilon^0$.

The functions F and G are readily evaluated numerically.

The final inverse temperature β is found by solving $E = 2J(N_{\rm nc} + N_\pi)$, or $N_\pi = \frac{J\rho_0 V}{4\pi^2}[G(\beta J)/2 - F(\beta J)]$. We find $N_\pi > 0$ if and only if $\beta J < 0.35$. This corresponds to $N > N^*$, where

$$N^* = 0.85\frac{JmV}{\hbar^2 d} = 0.85\rho_0 JV. \tag{8}$$

We conclude that if the initial number of bosons is greater than N^*, then the final state has a condensate, while if the initial number of bosons is smaller than N^*, then the final state does not have a condensate.

As one would expect, the threshold N^* is extensive. The condition $N = N^*$ can be understood by noting that the average transverse kinetic energy after relaxation is of order J, corresponding to a DeBroglie wavelength of order $\lambda = \hbar/\sqrt{2mJ}$. The threshold for condensation corresponds to when the average separation between particles in each 2D pancake is comparable to λ.

Interactions will somewhat move the threshold, but should not change the general behavior.

In the limit $N \gg N^*$, the fraction of noncondensed atoms becomes small. In that limit one can expand Eqs. (6) in powers of x (or βJ): $F(x) \to -(2\pi/x)\ln(x)$ and $G(x) \to 2\pi/x^2$. Thus, in this limit, the final temperature becomes very large compared to J: $\beta J \to \sqrt{\rho_0 VJ/(4\pi N)}$. The noncondensed fraction scales as $N_{\rm nc}/N \to N^{-1/2}\log N$ as $N \to \infty$.

Finite temperature

Our argument can be readily modified to account for thermal effects in the initial state.

Given an initial temperature β_0, the initial distribution of particles will be given by

$$f_{\epsilon_k^L}(\beta_0) = \frac{1}{e^{\beta_0\{\hbar^2 k_\perp^2/2m - J[1+\cos(k_z d)]\}} - 1}. \tag{9}$$

Since the occupations are based on the lower-band energies, this is very different than the equilibrium occupation of the higher band.

Given these occupations, the condensate number and the total energy after the quench are

$$N_0 = N - \int \frac{d^3k}{(2\pi)^3} f_{\epsilon_k^L}(\beta_0), \tag{10}$$

$$E = 2JN_0 + \int \frac{d^3k}{(2\pi)^3}\epsilon_k f_{\epsilon_k^L}(\beta_0). \tag{11}$$

As before, both number and energy are conserved in the dynamics, and the βJ describing the equilibrium distribution is found from Eq. (6), setting $N = N_{\rm nc} + N_\pi$ and $E = E_{\rm nc}$. In particular, N^* the threshold number of particles to find a condensate, is produced by setting $N_\pi = 0$.

Figure 2 shows how N^* varies with the initial temperature $\beta_0 J$. The result is nonmonotonic. When $k_B T_0 < J$, increasing the initial state temperature before quenching into the higher band actually reduces the total energy: Upper band atoms

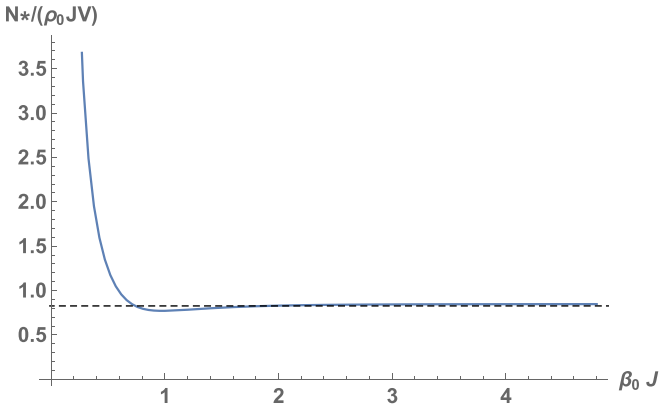

FIG. 2. Threshold N^* as a function of initial state temperature $\beta_0 J$. The dashed line shows N^* for $\beta_0 J \to \infty$.

with $k_z > 0$ have smaller energy than those with $k_z = 0$. This results in a smaller N^*.

Once $k_B T_0 > J$, further increasing the initial temperature in the lower band results in a higher upper-band energy: The relevant excitations are transverse to the lattice. This results in a larger N^*

Clearly, if $k_B T_0 < J$, then finite temperature effects are small, and it is reasonable to neglect them.

IV. HIGHER BAND KINETICS

Neglecting coherences between different momenta, one can use Fermi's golden rule to derive a quantum Boltzmann equation [32]. It is a standard practice to make an ergodic approximation [33–35], where all states of the same energy are taken to be equally occupied. This approximation postulates that equilibration between modes of same energy is fast compared to energy redistribution. We define $f(\varepsilon)$ (or f_ε) to be the occupation of modes with energy $\epsilon = J\varepsilon$. We separate out the mode with $k = 0$, defining $M = N_0/N$ to be the fraction of particles in that condensate. In Appendix C, we show

$$\frac{\partial f(\varepsilon_1)}{\partial \tilde{t}} = \frac{1}{\tilde{\rho}(\varepsilon_1)}\int \frac{d\varepsilon_2 d\varepsilon_3 d\varepsilon_4}{(2\pi)^3}\Pi_{34}^{12} 2\pi\delta(\varepsilon_1 + \varepsilon_2 - \varepsilon_3 - \varepsilon_4) \times [f_3 f_4(1+f_1)(1+f_2) - f_1 f_2(1+f_3)(1+f_4)] + 0.85\frac{N}{N^*}M^2(1+2f_1)\frac{\bar{\Gamma}}{(\varepsilon_1 - 2)^2 + (\bar{\Gamma}/2)^2}. \tag{12}$$

The second line corresponds to processes where two particles scatter out of the $k = 0$ condensate, while the first line includes processes where particles with energy ε_1 and ε_2 scatter into ε_3 and ε_4, or vice versa. Throughout, $f_j = f(\varepsilon_j)$, and the dimensionless density of state $\tilde{\rho}$ is defined in Eq. (7).

$$\int d\varepsilon\tilde{\rho}(\varepsilon)f(\varepsilon) = N_{\rm nc}/(\rho_0 JV) = 0.85N_{\rm nc}/N^*. \tag{13}$$

The rate of scattering out of the $k = 0$ condensate is parameterized by

$$\bar{\Gamma} = -0.85\frac{N/N^*}{\alpha}\frac{1}{M}\frac{dM}{d\tilde{t}} = 0.85\frac{N/N^*}{\alpha}M\int d\varepsilon\tilde{\rho}(\varepsilon)(1+2f(\varepsilon))\frac{\bar{\Gamma}}{(\varepsilon-2)^2 + (\bar{\Gamma}/2)^2}. \tag{14}$$

The Lorentzians in Eqs. (12) and (14) accounts for broadening due to the short condensate lifetime.

The dimensionless coefficient $\Pi_{34}^{12} = \Pi(\varepsilon_1, \varepsilon_2, \varepsilon_3, \varepsilon_4)$ is derived in Appendix D. Aside from a multiplicative factor of N^*/N, it only depends on the scaled energies, and no other parameters. When all scaled energies are smaller than 2, it reduces to a standard 3D result [36],

$$\Pi_{\varepsilon_{\max}<2} \propto \sqrt{\varepsilon_{\min}}, \tag{15}$$

where $\varepsilon_{\min}$ and $\varepsilon_{\max}$ are the smallest and largest of the ε_j. For large energies it becomes an elliptic function. We use an approximate form (explicitly given in the Appendix) which interpolates between these two expressions.

Times have been scaled, $\tilde{t} = t/\tau_N$, where

$$\tau_N = \frac{2\hbar V}{N\rho_0(Ud)^2} = \frac{2}{(4\pi)^2}\frac{d_a}{nd}\frac{1}{a_s^2}\frac{md_a}{\hbar}. \tag{16}$$

This scale can be interpreted as a microscopic collision time, $\tau_N \sim 1/(n_{\text{eff}}\sigma v)$, where $n_{\text{eff}} = nd/d_a$ is the effective density. The enhancement factor d_a/d reflects the fact that the Wannier states are compressed in one direction. The cross-section $\sigma = 4\pi a_s^2$ is proportional to the square of the scattering length. In this interpretation the characteristic velocity is proportional to $\hbar/md_a$. There are other possible velocities in the problem, and *a priori* it is not obvious which one to use. Nonetheless, Eq. (16) is a scaling which simplifies the equations.

In addition to N/N^*, there is only one other dimensionless parameter in these equations,

$$\alpha = \frac{N\tau_N}{\hbar V\rho_0} = 0.85\frac{J\tau_N}{\hbar}\frac{N}{N^*} = \frac{2}{(4\pi)^2}\left(\frac{d_a}{a_s}\right)^2. \tag{17}$$

The last expression is most transparent: recall, a_s is the scattering length, and d_a is the width of the Wannier states. Typically, $\alpha \sim 10$, though it can readily be increased or decreased by an order of magnitude by changing the lattice depth or employing a Feshbach resonance. In a given experiment, $\frac{N}{N^*}$ is varied by changing the number of atoms, or the lattice depth—see Eq. (8).

Our derivation breaks down if the condensate lifetime becomes significantly smaller than $\hbar/J$. In Sec. V A, we analyze the decay process, and find $\tau_{\text{decay}} \sim \tau_n/\sqrt{\alpha}$. Consequently, we require that α is not too small compared to $(N/N^*)^2$. Accurately modeling the small α limit would require keeping track of the coherences between the modes occupied during the evaporation process. Nonetheless, we expect our results to capture much of the physics, even in that limit.

V. RESULTS

We numerically integrate Eq. (12). The algorithmic details for this are in Appendix B. Figures 3(a) and 3(b) show typical time series for the $k = 0$ condensate fraction, the $k = \pi/d$ condensate fraction, and the width of the energy distribution $\Delta\varepsilon = \frac{N^*}{N}\sqrt{\int d\varepsilon\rho(\varepsilon)f(\varepsilon)(\varepsilon-2)^2}$. Four separate timescales are apparent: τ_{decay} is the timescale for decay of the $k = 0$ condensate; τ_{onset} is the characteristic time for the $k = \pi/d$ condensate to start growing, τ_{growth} is the timescale for the $k = \pi/d$ condensate to grow to its equilibrium value, and $\tau_E = J/[d(\Delta\varepsilon)/dt]$ is the inverse slope of the energy-width curve.

Numerically we find that $\tau_{\text{decay}} \sim \tau_N/\sqrt{\alpha}$, and $\tau_{\text{onset}} \sim \tau_{\text{growth}} \sim \tau_N N^*/N$, and $\tau_E \sim \tau_N$ (see Fig. 3(b,c,d,e). Thus when $\alpha \gg 1$ and $N > N^*$ there is a clear separation of scales. In Secs. V A, V B, and V C, we give analytic arguments for the scaling of the decay and growth processes.

A. Decay

The first stage of the dynamics, as illustrated in Fig. 3(a) is the decay of the $k = 0$ condensate. There, pairs of particles scatter to states whose energies are near $2J$.

To understand the scaling of this process as shown in Fig. 3(c), we neglect the first line of Eq. (12): As is verified by the numerics, the redistribution of energy amongst the noncondensed particles is slow compared to the evaporation. Throughout this initial stage, the function $f(\varepsilon)$ will be peaked about $\varepsilon = 2$, with height f_2 and width of order $\bar{\Gamma}$. Number conservation, Eq. (C22), implies that $f_2 \sim \frac{N}{N^*}(1-M)/\bar{\Gamma}$, where $M = N_0/N$ is the $k = 0$ condensate fraction. Recall that our arguments apply when α is large, and hence the rate $1/\tau_{\text{evap}} = J\bar{\Gamma}/(\hbar)$ will be small. Thus, f_2 will be large compared to 1, and in Eq. (12) we can replace $1 + 2f \approx 2f$. The integrand in Eq. (14) will have height $f_2/\bar{\Gamma}$, and width $\bar{\Gamma}$, and hence the integral is of order f_2. Thus one expects $\bar{\Gamma} \sim \frac{N/N^*}{\sqrt{\alpha}}\sqrt{M(1-M)}$, as long as M is not too close to 1. The characteristic timescale for decay of the $k = 0$ condensate is found by taking $M(1-M)$ to be of order 1, which yields $\tau_{\text{evap}} = \hbar/(J\bar{\Gamma}) \sim \tau_N/\sqrt{\alpha}$.

B. Energy redistribution

The second stage of the dynamics, as seen in Fig. 3(b), is the redistribution of energy among the noncondensed particles. At short and intermediate times, the energy-width of the distribution function grows roughly linearly in time. The slope of this curve is of order J/τ_N, consistent with the fact that the typical energy is $2J$ and the characteristic scattering time is τ_N. The energy-width saturates at long time. The timescale for saturation is roughly the onset time for growth of the $k = \pi/d$ condensate.

C. Growth

The scaling of the onset and growth times as seen in Figs. 3(d) and 3(e) both are consequences of Bose stimulation. Once the $k = 0$ condensate evaporates, the noncondensed particles redistibute their energies. A microscopic seed forms at $k = \pi/d$ in a time of order τ_N. The number of particles in that seed will scale linearly with the density, and will therefore be proportional to N. This seed then grows exponentially, and the time that it takes to become macroscopic will be inversely proportional to the initial number. Hence, $\tau_{\text{onset}} \sim \tau_N N^*/N$. The timescale for growth will also scale in this manner.

VI. DECAY TO THE LOWER BAND

Our analysis is predicated on the dynamics within the band being fast compared to the interband decay. Here we

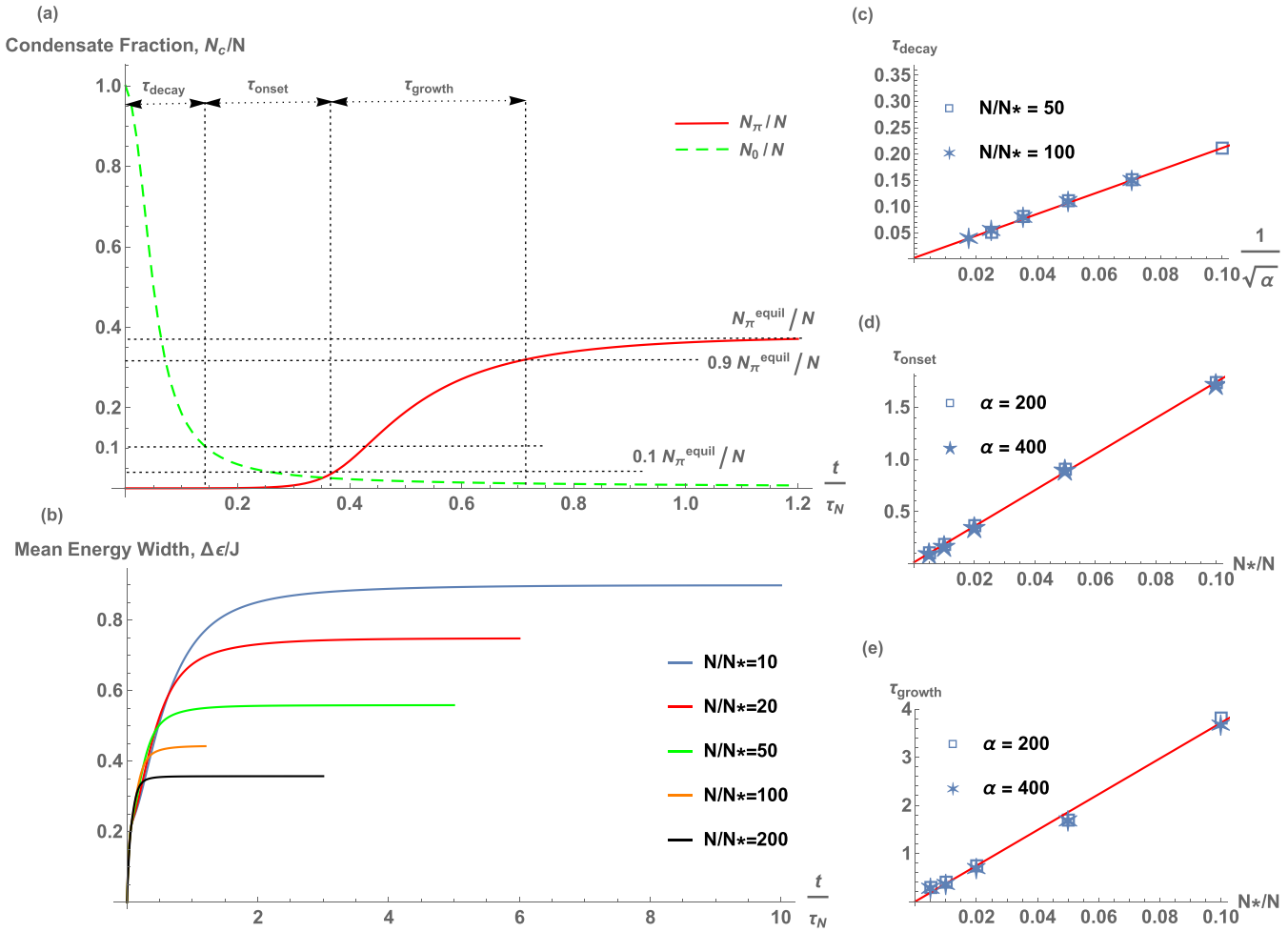

FIG. 3. (a) Fraction of particles in $k_z = 0$ condensate (green, dashed) and $k_z = \pi$ condensate (red, solid) plotted against dimensionless time, t/τ_N for $N/N^* = 100$ and $\alpha = 200$. Three different timescales can be seen: τ_{decay}, the decay of $k_z = 0$ condensate; τ_{onset}, onset of formation of $k_z = \pi/d$ condensate; and τ_{growth}, the growth of $k_z = \pi/d$ condensate. (b) Mean energy width, $\Delta\epsilon/J$ of the distribution functions, $f(\varepsilon)$ versus t/τ_N for different N/N^* values with $\alpha = 200$. N/N^* increases from top to bottom. (c) $\tau_{\text{decay}}/\tau_N$, (d) $\tau_{\text{onset}}/\tau_N$, (e) $\tau_{\text{growth}}/\tau_N$.

estimate that decay rate, finding that the ratio of the interband and intraband rates is proportional to $(J'/\Delta)^2$. Since in the experiments $(J'/\Delta) \ll 1$ [12], there is a large separation of scales.

This suppression comes from the poor spatial overlap between the upper-band wave functions (which are predominantly on the A sublattice) and the lower band wave functions (predominantly on B).

The loss of atoms from the condensate in the upper band at $\mathbf{k} = \pi$ to the lower band is driven by the interaction term [37], and the rate can be calculated using Fermi's golden rule. The leading process involves two upper band $k = \pi$ atoms scattering to produce a lower band atom with momentum k, and an upper band atom with momentum k'. Using the dispersion calculated in Appendix (A), the energy of this final state only depends on the transverse momentum, $\epsilon_f = -\Delta + 2\hbar^2 k_\perp^2/2m$. The matrix element is calculated by substituting the operators for the Bloch states from Appendix A into the interaction Hamiltonian. Taking $N_\pi \approx N \gg 1$ and assuming that none of the lower band states are macroscopically occupied, we can repeat the argument in Appendix C 1 b that we used to calculate intraband decays, and find

$$\Gamma_{ab} = \frac{-1}{N_\pi}\frac{dN_\pi}{dt} = \frac{2\pi}{\hbar}\sum_f |\langle\psi_f|H_{\text{int}}|\psi_i\rangle|^2\delta(\epsilon_f - \epsilon_i).$$
$$= \frac{N}{V\hbar}\int\frac{d^3k}{(2\pi)^2}\left(\frac{2J'U_a\cos(k_z d/2)}{\Delta}\right)^2\delta\left(\frac{\hbar^2k_\perp^2}{m} - \Delta\right).$$
$$= \left(\frac{2J'}{\Delta}\right)^2\frac{NmdU_a^2}{2V\hbar^3} = \left(\frac{2J'}{\Delta}\right)^2\frac{1}{\tau_N}. \quad (18)$$

As already explained, the factor $(2J'/\Delta)^2$ is typically much much smaller than 1, implying that the decay from the higher band ($\tau_{\text{ab}} \sim 1/\Gamma_{\text{ab}}$) is slow compared to the kinetics within the higher band.

VII. EXPERIMENTAL SIGNATURE

A direct way to verify these kinetics is to experimentally measure the time-dependent momentum distribution through time-of-flight (TOF) expansion. After free expansion for time

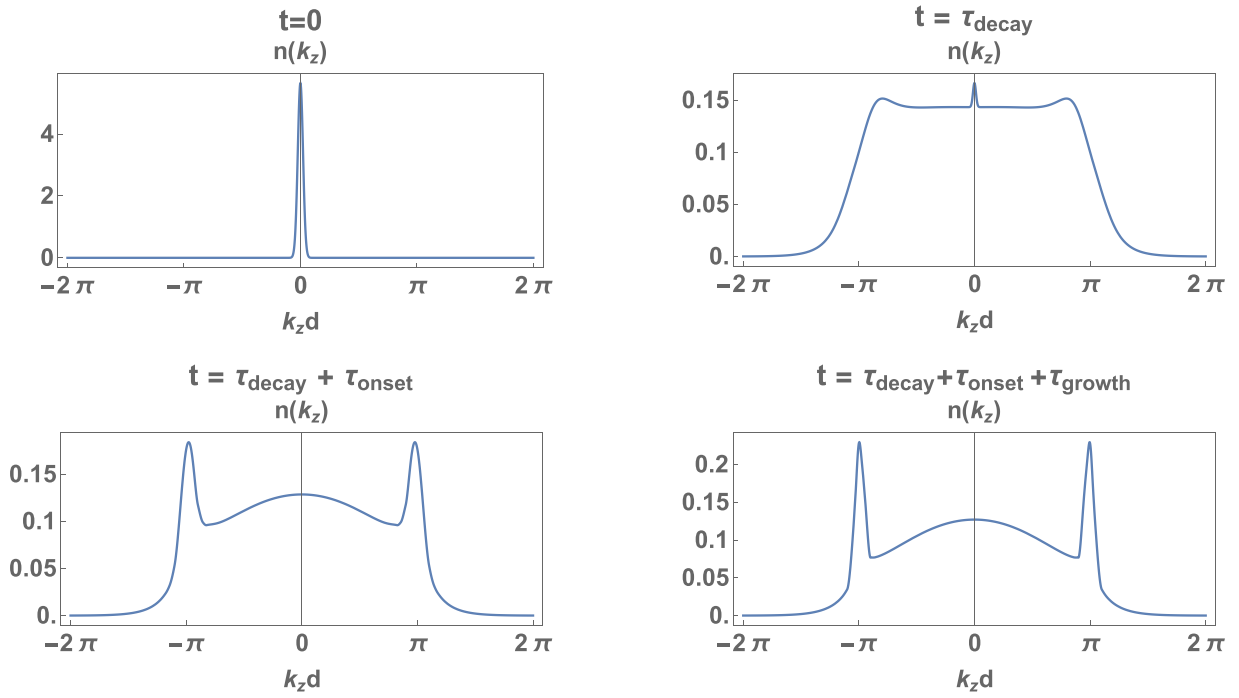

FIG. 4. Simulated time-of-flight images showing momentum space density of atoms along k_z for $N/N^* = 100$ and $\alpha = 200$. (Area under the curves has been normalized to 1 in the figure) The $t = 0$ image represents time just after the quench and then the time-of-flight expansion is shown for elapsed times, $t = \tau_{\text{decay}}$, $t = \tau_{\text{decay}} + \tau_{\text{onset}}$ and $t = \tau_{\text{decay}} + \tau_{\text{onset}} + \tau_{\text{growth}}$, corresponding to the dotted vertical lines in Fig. 3(a),

τ one measures the column-density of atoms,

$$n^c_{\text{TOF}}(z) = \int dxdy\, n_{\text{TOF}}(\mathbf{r}). \tag{19}$$

Defining $k_z = mz/(\hbar\tau)$, the column density is related to the *in situ* momentum density of the trapped atoms at the time of release [38], t,

$$n_{\text{TOF}} \propto |w(k_z)|^2 \int dk_x dk_y\, n_{\text{trap}}(\mathbf{k}, t) \tag{20}$$

$$= |w(k_z)|^2 \int_{J(1+\cos k_z d)}^{\infty} d\epsilon\, f(\epsilon, t) + |w(0)|^2 N_0(t)\delta(k_z). \tag{21}$$

Here $w(k)$ is the Fourier transform of the Wannier function in the lattice, and when it is an argument of the distribution function, k_z is projected into the Brillioun zone.

We numerically integrate the distribution functions calculated from Eq. (12). Figure 4 shows the expected time-of-flight images at different times. During the evaporation phase, the image is dominated by a δ-function peak at $k_z = 0$. In an experiment this peak has a nonzero width, set by the finite system size and the finite expansion time. In Fig. 4, we use a Gaussian of width $0.01k_z d$. As the condensate evaporates, a halo representing the noncondensed particles appears. As the particles redistribute themselves, structures form, and well before a $k_z = \pi/d$ condensate appears, one sees peaks near $k_z = \pi/d$. These peaks sharpen over time as phase coherence develops on longer length scales. A true condensate at $k_z = \pi/d$ would be characterized by δ-function peaks. Again, finite system size and expansion time would spread out these δ functions. In our numerics the sharpness is limited by the resolution of our discretization of the energy.

For the plots in Fig. 4, we use a Gaussian Wannier state corresponding to a lattice depth of $5E_R$ where E_R is the recoil energy. We choose $N/N^* = 100$ and $\alpha = 200$

VIII. BEYOND UPPER BANDS

As already discussed, our model can be used in settings other than the upper band of an optical lattice. One example is the experiments of Lignier *et al.* from Pisa [30] where an optical lattice loaded with a condensate is sinusoidally shaken to dynamically change the tunneling amplitude J between nearest-neighboring sites. They can flip the sign of the effective tunneling amplitude and invert the band. This situation is similar to our model where the condensate is promoted to the higher band.

In that experiment, the optical lattice has a spacing of 426 nm and is loaded with Rb-87 atoms. The lattice depth is about $9E_R$ where E_R is the recoil energy of the lattice. The number density is of the order $10^{14}\,\text{cm}^{-3}$, which is typical of cold gas condensates and the s-wave scattering length between the atoms is about 5 nm. The timescale τ_N that we get from these parameters would be about 10 ms. While the published data does not include a detailed study of timescales, our estimate is consistent with the observation of a double peak structure in time of flight after a few ms. Other single band realizations are likely to have similar parameters.

IX. SUMMARY

We modeled the dynamics of a nonequilibrium condensate formed in the highest energy state of an excited band in an

optical lattice. We find that there is a critical particle number, below which the final state has no condensate. We derive kinetic equations and use them to calculate the time-dynamics of this system. We find three distinct timescales: a fast timescale over which the initial condensate evaporates, an intermediate timescale over which collisions occur, and slower timescale over which a condensate grows. This scenario is very different from more conventional paradigms of order parameter dynamics, for example involving an order parameter "rolling down" a potential hill [1] or evolving through a modulational instability [39,40]. This kinetic path is likely important in other experiments such as those involving shaken lattices [16–19] or soliton formation [41].

We show how these processes can be seen in time-of-flight expansion images, allowing a direct experimental verification of our predictions.

ACKNOWLEDGMENTS

This material is based upon work supported by the National Science Foundation under Grant No. PHY-1806357 and the ARO-MURI Non-equilibrium Many-body Dynamics Grant No. W9111NF-14-1-0003.

APPENDIX A: DERIVATION OF OPERATORS FOR BLOCH EIGENSTATES AND BAND DISPERSIONS

Here we explicitly give the momentum-space representation of the single-particle Hamiltonian in Eq. (1).

The real-space Hamiltonian is given in Eq. (1). We define momentum space field operators by

$$a_j(\mathbf{r}_\perp) = \sqrt{Vd}\int \frac{d^3k}{(2\pi)^3} a_k e^{i(\mathbf{k}_\perp\cdot\mathbf{r}_\perp + jk_z d)}. \tag{A1}$$

Analogous expressions relate $b_j(\mathbf{r}_\perp)$ and b_k. Here, and in similar equations from the main text, the integral is over all $\mathbf{k}_\perp$, but $-\pi/d < k_z < \pi/d$, and V is the volume of the system. The length of the unit cell in the z direction is d. Substituting these relations into the Hamiltonian yields (for $t > 0$)

$$H = V\int \frac{d^3k}{(2\pi)^3}(a_{\mathbf{k}}^\dagger \quad b_{\mathbf{k}}^\dagger) H_k \begin{pmatrix} a_{\mathbf{k}} \\ b_{\mathbf{k}} \end{pmatrix}, \tag{A2}$$

$$H_{\mathbf{k}} = \begin{pmatrix} \frac{\hbar^2 k_\perp^2}{2m} & -2J'\cos(k_z d/2) \\ -2J'\cos(k_z d/2) & \frac{\hbar^2 k_\perp^2}{2m} - \Delta \end{pmatrix}. \tag{A3}$$

In the experimentally relevant regime, $\Delta \gg J'$, the dispersion relation for the upper and lower band, respectively, are given by

$$\epsilon_{\mathbf{k}}^H = J[1+\cos(k_z d)] + \frac{\hbar^2 k_\perp^2}{2m}, \tag{A4}$$

$$\epsilon_{\mathbf{k}}^L = -\Delta - J[1+\cos(k_z d)] + \frac{\hbar^2 k_\perp^2}{2m}, \tag{A5}$$

where $J = 2(J')^2/\Delta$. The eigenstates for higher and lower band, respectively, are given by

$$|\psi(k)\rangle^H = \overline{a}_k^\dagger|0\rangle \approx \left[a_k^\dagger - \frac{2J'\cos(k_z d/2)}{\Delta} b_k^\dagger\right]|0\rangle, \tag{A6}$$

$$|\psi(k)\rangle^L = \overline{b}_k^\dagger|0\rangle \approx \left[b_k^\dagger + \frac{2J'\cos(k_z d/2)}{\Delta} a_k^\dagger\right]|0\rangle. \tag{A7}$$

Before the quench, the system is condensed in a state of the same form as Eq. (A6), but with $\Delta \to -\Delta$. Since the overlap between these states are near unity, the quench projects the condensate into the higher band.

APPENDIX B: DISCRETIZATION

To numerically integrate Eqs. (12) and (14), we discretize energy and time, using bin sizes $\delta\varepsilon$ and $\delta\tilde{t}$. Integrals over ε become sums, and we evaluate functions of ε at the midpoint of each bin. We used both an Euler method and a fourth order Runge-Kutta method for our time-stepping. We chose our time step so that the estimated temporal discretization error is at the subpercent level. We use $\varepsilon_{\max} = 20$ as our largest bin, and verified that the resulting errors were on the percent level.

The temporal scaling with the number of energy bins N_ε is poor, with each evaluation of the integrals in Eq. (C13) taking a time that scales as N_ε^3. We calculate the kinetics with $\delta\varepsilon = 0.1, 0.05, 0.025$, and 0.0125 corresponding to $N_\varepsilon = 200, 400, 800, 1600$.

We use the number of atoms in our smallest energy bin as a proxy for the number of atoms condensed at $k = \pi$. In equilibrium, this approach overestimates the number of condensed particles by a factor which scales with $\sqrt{\delta\varepsilon}$. To correct for this factor, we run our simulation with multiple values of $\delta\varepsilon$ and extrapolate to $\delta\varepsilon \to 0$.

APPENDIX C: DERIVATION OF BOLTZMANN EQUATION

Following standard arguments [32], we begin with Fermi's Golden Rule, and write the rate of change of the occupation of the mode with momentum k as

$$\frac{\partial N_k}{\partial t} = \sum_f |\langle f|H_{\rm int}|i\rangle|^2 \left(N_k^f - N_k^i\right)\frac{2\pi}{\hbar}\delta(E_f - E_i), \tag{C1}$$

where the states $|i\rangle$ and $|f\rangle$ have definite numbers of particles in each momentum state. Here N_k^i and N_k^f are the initial and final number of particles in state k. The energy of each state is E_i and E_f.

The interaction Hamiltonian involves taking particles with momentum k_1 and k_2 scatter into k_3 and $k_4 = k_1 + k_2 - k_3$. In particular, we use the interactions from Eq. (5),

$$H_{\rm int} = \frac{U}{2}\frac{d}{V}\sum_{k_1k_2k_3} a_{\mathbf{k_1}+\mathbf{k_2}-\mathbf{k_3}}^\dagger a_{\mathbf{k_3}}^\dagger a_{\mathbf{k_2}} a_{\mathbf{k_1}}. \tag{C2}$$

1. Explicit kinetic equations

a. Noncondensed contributions

We will first consider the terms not involving condensates—for which k_1, k_2, k_3, and k_4 can be taken as distinct. There are four terms in Eq. (C2) which connect i to f, corresponding to permuting the various indices. The sum of these four equal contributions yields

$$\langle f|H_{\rm int}|i\rangle = \frac{2Ud}{V}\sqrt{N_1}\sqrt{N_2}\sqrt{1+N_3}\sqrt{1+N_4}, \tag{C3}$$

where we have used the shorthand $N_j = N_{k_j}$. Thus, the contribution to $\partial N_k/\partial t$ from these terms are

$$\frac{\partial N_k^{(1)}}{\partial t} = \frac{2U^2d^2}{\hbar}\int\frac{d^3q\,d^3k'}{(2\pi)^6}\Upsilon\,2\pi\delta(\epsilon_k+\epsilon_{k'}-\epsilon_{k-q}-\epsilon_{k'+q}),$$
$$\Upsilon = [N_{k-q}N_{k'+q}(1+N_k)(1+N_{k'}) - N_kN_{k'}(1+N_{k-q})(1+N_{k'+q})]. \quad \text{(C4)}$$

The superscript (1) indicates that we have not yet included the condensate contributions.

b. Condensate contributions

In the presence of a condensate, we also have to separately consider terms where two atoms scatter out of the condensate, or the reverse. There is no way to conserve energy and scatter two particles into or out of $k = \pi$, so we only need to worry about such terms for the condensate at $k = 0$. Thus we take $|f\rangle$ to differ from $|i\rangle$ by having two fewer particles with momenta $k = 0$, and two more particle with momenta, respectively, q and $-q$. The matrix element is

$$\langle f|H_{\rm int}|i\rangle = \frac{Ud}{V}\sqrt{N_0-1}\sqrt{N_0}\sqrt{1+N_q}\sqrt{1+N_{-q}}, \quad \text{(C5)}$$

Note the factor of 2 different from Eq. (C3), as there are only two terms in $H_{\rm int}$ which contribute, instead of 4. The net result is

$$\frac{\partial N_0}{\partial t} = (Ud)^2\frac{N_0^2}{\hbar V}\int\frac{d^3q}{(2\pi)^3}\bar{\Upsilon}\,2\pi\tilde{\delta}(2\epsilon_q-2\epsilon_0),$$
$$\bar{\Upsilon} = [N_qN_{-q}-(1+N_q)(1+N_{-q})],$$
$$\frac{\partial N_q^{(2)}}{\partial t} = \frac{U^2d^2N_0^2}{\hbar V^2}(1+N_q+N_{-q})\,2\pi\tilde{\delta}(2\epsilon_q-2\epsilon_0), \quad \text{(C6)}$$

where we have assumed $N_0 \gg 1$. The superscript (2) indicates that we are only considering the condensate contributions. In the standard derivation of the quantum Boltzmann equation, $\tilde{\delta}$ is simply a Dirac δ function. For the decay of the condensate, the finite condensate lifetime is important, so we take

$$2\pi\tilde{\delta}(2\epsilon) = \frac{2\hbar\Gamma}{(2\epsilon)^2+(\hbar\Gamma)^2}. \quad \text{(C7)}$$

The decay rate Γ should be calculated self-consistently:

$$\Gamma = -\frac{1}{N_0}\frac{\partial N_0}{\partial t}. \quad \text{(C8)}$$

c. Further considerations—Necessity of self-consistently including the lifetime of the condensate mode

It is crucial that the δ function in Eq. (C6) is replaced by a Lorentzian—for otherwise, one gets incorrect results.

To understand this necessity, consider solving Eq. (C6) in the absence of the redistribution terms in Eq. (C4). Further imagine treating Γ as a constant, rather than self-consistently solving for it. The standard approach of neglecting the broadening would correspond to taking the limit $\Gamma \to 0$.

Under these circumstances, condensate decay only occurs into modes where $|\epsilon_q - \epsilon_0|$ is no greater than Γ. There are roughly $V\rho_0\Gamma$ of these, where $\rho_0 = m/(\hbar^2 d)$ is the density of states per unit volume. Thus the average occupation of a mode will be of order $N_q \sim \hbar^2 nd/(m\Gamma)$. If this becomes larger than 1, then Bose-enhancement is important for setting the rate of decay. In particular, if $\Gamma \to 0$, then the decay rate becomes infinitely fast. This is clearly unphysical.

As already presented, the correct way to control this divergence is to find $\Gamma(t)$ self-consistently.

d. Limits of validity

If the condensate decay rate Γ becomes large compared to the bandwidth $2J$, then quantum coherent effects need to be included: The single-particle states become strongly hybridized, and the quantum state is no longer well characterized by just specifying the occupations of different k modes. Therefore we will require $\Gamma \ll 2J$. As discussed in the main text, this requirement means that our approach is only accurate for sufficiently large α.

2. Ergodic approximation and adimensionalizing

We make the ergodic approximation, where all states with the same energy are taken to be equally occupied: $N_k = f(\epsilon_k)$. We convert our expressions into equations for $f(\epsilon)$ by using

$$\int\frac{d^3k}{(2\pi)^3}\frac{\partial N_k}{\partial t}2\pi\delta(\epsilon-\epsilon_k) = \frac{1}{V}\rho(\epsilon)\frac{\partial f(\epsilon)}{\partial t}. \quad \text{(C9)}$$

After making the ergodic approximation, we adimensionalize our equations. We measure times in terms of

$$\tau_N = \frac{2\hbar V}{N\rho_0(Ud)^2}, \quad \text{(C10)}$$

denoting $\tilde{t} = t/\tau_N$. For the kinetic processes in Eq. (C4) we find it convenient to rescale energies by J, writing $\varepsilon = \epsilon/J$. We further adimensionalize momenta by rescaling, $k_z = q_z/d$, and $\mathbf{k}_\perp = \mathbf{q}_\perp/\sqrt{\hbar^2/2mJ}$.

In terms of these variables, Eq. (C4) becomes

$$\frac{\partial f^{(1)}(\varepsilon_1)}{\partial\tilde{t}} = \frac{1}{\tilde{\rho}(\varepsilon_1)}\int\frac{d\varepsilon_2 d\varepsilon_3 d\varepsilon_4}{(2\pi)^3}M_{34}^{12}\Pi_{34}^{12}\bar{\Delta}, \quad \text{(C11)}$$

where energy conservation comes from

$$\bar{\Delta} = 2\pi\delta(\varepsilon_1+\varepsilon_2-\varepsilon_3-\varepsilon_4). \quad \text{(C12)}$$

The occupation numbers enter in the coefficient

$$M_{34}^{12} = f_3f_4(1+f_2)(1+f_1) - f_1f_2(1+f_3)(1+f_4), \quad \text{(C13)}$$

where $f_j = f(\varepsilon_j)$. The dimensionless matrix element is

$$\Pi_{34}^{12} = A\int Dk\;\Delta_1\Delta_2\Delta_3\Delta_4K_{1234}, \quad \text{(C14)}$$

where

$$A = 32\frac{N^*}{0.85N}, \quad \text{(C15)}$$

$$Dk = \frac{d^3q_1}{(2\pi)^3}\frac{d^3q_2}{(2\pi)^3}\frac{d^3q_3}{(2\pi)^3}\frac{d^3q_4}{(2\pi)^3}, \quad \text{(C16)}$$

$$\Delta_j = 2\pi\delta[\varepsilon_j - \varepsilon(q_j)], \quad \text{(C17)}$$

$$K_{1234} = (2\pi)^3\delta^3(q_1+q_2-q_3-q_4) \quad \text{(C18)}$$

are, respectively, the amplitude, measure, energy conserving δ functions, and a momentum conserving δ function. In Appendix D we approximate Eq. (C14) as

$$\frac{\Pi_{34}^{12}}{A} \approx \frac{1}{\frac{64\pi^2}{\sqrt{\varepsilon_2}} + \frac{2\pi(\varepsilon_3\varepsilon_4)^{1/2}}{K[\varepsilon_1\varepsilon_2/(\varepsilon_3\varepsilon_4)]}}, \tag{C19}$$

which is exact for both high energy and low energy collisions, and is numerically efficient to calculate.

After rescaling, Eq. (C6) becomes

$$\frac{df(\varepsilon)}{d\tilde{t}} = 0.85\frac{N}{N^*}M^2(1+2f(\varepsilon))\frac{\bar{\Gamma}}{(\varepsilon-2)^2+(\bar{\Gamma}/2)^2}, \tag{C20}$$

$$\bar{\Gamma} = -0.85\frac{N/N^*}{\alpha}\frac{1}{M}\frac{dM}{d\tilde{t}} = 0.85\frac{N/N^*}{\alpha}M\int d\varepsilon\frac{\tilde{\rho}(\varepsilon)(1+2f(\varepsilon))\bar{\Gamma}}{(\varepsilon-2)^2+(\bar{\Gamma}/2)^2}, \tag{C21}$$

where $M = N_0/N$. We have assumed the condensate fraction is large, $N_0 \gg 1$.

$\bar{\Gamma} = \hbar\Gamma/J$ is the adimensionalized condensate evaporation rate. Number conservation is cast as

$$M + \frac{1}{0.85N/N^*}\int \tilde{\rho}(\varepsilon)f(\varepsilon)\,d\varepsilon = 1. \tag{C22}$$

APPENDIX D: DIMENSIONLESS MATRIX ELEMENT Π_{12}^{34}

Here we calculate the matrix element in Eq. (C11).

1. Low-energy limit

We first evaluate the matrix element integral in the low energy limit where all of the energies have $\varepsilon \ll 1$. In that case one can expand about the minimum, and it becomes a standard 3D gas calculation. In particular, shifting the origin and using dimensionless energy and momenta,

$$\varepsilon(k) \approx k_\perp^2 + k_z^2. \tag{D1}$$

We first go to the center of mass frame in momentum for Eq. (C14) to get

$$\Pi_{34}^{12} = A\int\frac{d^3K}{(2\pi)^3}\int\frac{d^3q}{(2\pi)^3}\int\frac{d^3q'}{(2\pi)^3}\delta_1\delta_2\delta_3\delta_4, \tag{D2}$$

where

$$q_1 = K/2 + q, \tag{D3}$$

$$q_2 = K/2 - q, \tag{D4}$$

$$q_3 = K/2 + q', \tag{D5}$$

$$q_4 = K/2 - q', \tag{D6}$$

$$\delta_1 = 2\pi\delta(\varepsilon_1 - |K/2+q|^2), \tag{D7}$$

$$\delta_2 = 2\pi\delta(\varepsilon_2 - |K/2-q|^2), \tag{D8}$$

$$\delta_3 = 2\pi\delta(\varepsilon_3 - |K/2+q'|^2), \tag{D9}$$

$$\delta_4 = 2\pi\delta(\varepsilon_4 - |K/2-q'|^2). \tag{D10}$$

Next we transform to spherical coordinates, letting θ be the angle between K and q, and θ' be the angle between K and q'. We can do the angular integrals followed by the q and q' integrals to get

$$\Pi_{34}^{12} = \frac{A}{16}\frac{1}{(2\pi)^2}\int dK\theta_1\theta_2\theta_3\theta_4, \tag{D11}$$

where

$$\begin{aligned}
\theta_1 &= \theta\left(\left[\frac{\varepsilon_1+\varepsilon_2}{2} - \frac{K^2}{4}\right]K^2 - \left[\frac{\varepsilon_1-\varepsilon_2}{2}\right]^2\right),\\
\theta_2 &= \theta\left(\left[\frac{\varepsilon_3+\varepsilon_4}{2} - \frac{K^2}{4}\right]K^2 - \left[\frac{\varepsilon_3-\varepsilon_4}{2}\right]^2\right),\\
\theta_3 &= \theta(\varepsilon_1+\varepsilon_2-K^2/2),\\
\theta_4 &= \theta(\varepsilon_3+\varepsilon_4-K^2/2),
\end{aligned} \tag{D12}$$

where throughout $\theta(x)$ is the Heaviside step function (equal to 1 when $x > 0$ and otherwise zero). The integrand in Eq. (D11) is always zero or 1. The latter occurs when

$$|\sqrt{\varepsilon_1} - \sqrt{\varepsilon_2}| < K < \sqrt{\varepsilon_1} + \sqrt{\varepsilon_2}, \tag{D13}$$

$$|\sqrt{\varepsilon_3} - \sqrt{\varepsilon_4}| < K < \sqrt{\varepsilon_3} + \sqrt{\varepsilon_4}, \tag{D14}$$

$$K < \sqrt{2}\sqrt{\varepsilon_1+\varepsilon_2}, \tag{D15}$$

$$K < \sqrt{2}\sqrt{\varepsilon_3+\varepsilon_4}. \tag{D16}$$

It is convenient to write

$$\varepsilon_1 = \bar{\varepsilon} + \delta, \tag{D17}$$

$$\varepsilon_2 = \bar{\varepsilon} - \delta, \tag{D18}$$

$$\varepsilon_3 = \bar{\varepsilon} + \delta', \tag{D19}$$

$$\varepsilon_4 = \bar{\varepsilon} - \delta'. \tag{D20}$$

Let us further assume that $\delta > \delta' > 0$. That means that $\epsilon_2 < \epsilon_4 < \epsilon_3 < \epsilon_1$. Consequently,

$$|\sqrt{\varepsilon_1} - \sqrt{\varepsilon_2}|^2 = 2\bar{\varepsilon} - \sqrt{\bar{\varepsilon}^2 - \delta^2} \tag{D21}$$

$$> 2\bar{\varepsilon} - \sqrt{\bar{\varepsilon}^2 - (\delta')^2} \tag{D22}$$

$$= |\sqrt{\varepsilon_3} - \sqrt{\varepsilon_4}|^2 \tag{D23}$$

and

$$|\sqrt{\varepsilon_1} + \sqrt{\varepsilon_2}|^2 = 2\bar{\varepsilon} + \sqrt{\bar{\varepsilon}^2 - \delta^2} \tag{D24}$$

$$< 2\bar{\varepsilon} + \sqrt{\bar{\varepsilon}^2 - (\delta')^2} \tag{D25}$$

$$= |\sqrt{\varepsilon_3} + \sqrt{\varepsilon_4}|^2. \tag{D26}$$

Hence, the integral is just

$$\Pi_{34}^{12} = \frac{A}{16}\frac{1}{(2\pi)^2}\sqrt{\varepsilon_2}. \tag{D27}$$

Of course, this result was predicated on ϵ_2 being the smallest energy. More generally, we have

$$\Pi_{34}^{12} = \frac{A}{16}\frac{1}{(2\pi)^2}\text{Min}(\sqrt{\varepsilon_1}, \sqrt{\varepsilon_2}, \sqrt{\varepsilon_3}, \sqrt{\varepsilon_4}). \quad \text{(D28)}$$

This is a well-known classic result in kinetic theory [36].

2. High energy

Next we consider the case where all of the ε's are large compared to 1. We can then approximate

$$\varepsilon(k) \approx k_\perp^2, \quad \text{(D29)}$$

and neglect the k_z dependence. All momenta here are dimensionless. We do the k_z integrals and scale and recenter the momenta as in Eq. (D2) to arrive at

$$\Pi_{34}^{12} = A\int \frac{d^2K}{(2\pi)^2}\int \frac{d^2q}{(2\pi)^2}\int \frac{d^2q'}{(2\pi)^2}\delta_1\delta_2\delta_3\delta_4. \quad \text{(D30)}$$

We transform to polar coordinates, letting θ be the angle between K and q, and θ' be the angle between K and q'. Doing the angular integral first, followed by the integral over q and q', we get

$$\Pi_{34}^{12} = \frac{A}{16}\int \frac{d(K^2)}{4\pi}\frac{1}{\sqrt{f(K)}}\frac{1}{\sqrt{g(K)}}, \quad \text{(D31)}$$

where

$$f(K) = \left(\frac{\varepsilon_1+\varepsilon_2}{2} - \frac{K^2}{4}\right)K^2 - \left(\frac{\varepsilon_1-\varepsilon_2}{2}\right)^2, \quad \text{(D32)}$$

$$g(K) = \left(\frac{\varepsilon_3+\varepsilon_4}{2} - \frac{K^2}{4}\right)K^2 - \left(\frac{\varepsilon_3-\varepsilon_4}{2}\right)^2. \quad \text{(D33)}$$

Here the integral is taken over the domain where the arguments of the square roots are positive. We know from our previous arguments that if we take $\varepsilon_2 < \varepsilon_4 < \varepsilon_3 < \varepsilon_1$ then $K_{\text{min}} = \sqrt{\varepsilon_1} - \sqrt{\varepsilon_2}$ and $K_{\text{max}} = \sqrt{\varepsilon_1} + \sqrt{\varepsilon_2}$, or $K_{\text{min}}^2 = \varepsilon_1 + \varepsilon_2 - 2\sqrt{\varepsilon_1\varepsilon_2}$ and $K_{\text{max}}^2 = \sqrt{\varepsilon_1} + \sqrt{\varepsilon_2} + 2\sqrt{\varepsilon_1\varepsilon_2}$.

Equation (D31) is an elliptic integral. To show that, we factor the expressions in the square roots, to get

$$\Pi_{34}^{12} = \frac{A}{16\pi}\int dK^2 \frac{1}{\sqrt{p_1p_2p_3p_4}}, \quad \text{(D34)}$$

where

$$p_1 = (K^2 - 2\bar{\varepsilon} - 2\sqrt{\varepsilon_1\varepsilon_2}), \quad \text{(D35)}$$

$$p_2 = (K^2 - 2\bar{\varepsilon} + 2\sqrt{\varepsilon_1\varepsilon_2}), \quad \text{(D36)}$$

$$p_3 = (K^2 - 2\bar{\varepsilon} - 2\sqrt{\varepsilon_3\varepsilon_4}), \quad \text{(D37)}$$

$$p_4 = (K^2 - 2\bar{\varepsilon} - 2\sqrt{\varepsilon_3\varepsilon_4}), \quad \text{(D38)}$$

where $\bar{\varepsilon} = (\varepsilon_1+\varepsilon_2)/2 = (\varepsilon_3+\varepsilon_4)/2$. We then shift and rescale K^2, writing

$$s = \frac{K^2 - 2\bar{\varepsilon}}{2\sqrt{\varepsilon_1\varepsilon_2}} \quad \text{(D39)}$$

to find

$$\Pi_{34}^{12} = \frac{A}{4\pi}\frac{1}{\sqrt{\varepsilon_1\varepsilon_2}}\int_{-1}^{1}\frac{ds}{\sqrt{(s^2-1)\left(s^2 - \frac{\varepsilon_2\varepsilon_3}{\varepsilon_1\varepsilon_2}\right)}}. \quad \text{(D40)}$$

This is the Jacobi notation for the complete Elliptic Integral of the first kind,

$$K(1/t) = \frac{\sqrt{t}}{2}\int_{-1}^{1}\frac{ds}{\sqrt{(s^2-1)(s^2-t)}}, \quad \text{(D41)}$$

which gives

$$\Pi_{34}^{12} = \frac{A}{2\pi}\frac{1}{\sqrt{\varepsilon_3\varepsilon_4}}K\left(\frac{\varepsilon_1\varepsilon_2}{\varepsilon_3\varepsilon_4}\right). \quad \text{(D42)}$$

By construction, $\varepsilon_1\varepsilon_2 < \varepsilon_3\varepsilon_4$. More generally,

$$\Pi_{34}^{12} = \frac{A}{2\pi}\frac{1}{\sqrt{E_2}}K\left(\frac{E_1}{E_2}\right), \quad \text{(D43)}$$

where $E_1 = \min(\varepsilon_1\varepsilon_2, \varepsilon_3\varepsilon_4)$, and $E_2 = \max(\varepsilon_1\varepsilon_2, \varepsilon_3\varepsilon_4)$.

3. Interpolation

To connect these two limits we use a simple interpolation,

$$\Pi_{12}^{34} = \frac{A}{\frac{64\pi^2}{\sqrt{\varepsilon_2}} + \frac{2\pi(\varepsilon_3\varepsilon_4)^{1/2}}{K[\varepsilon_1\varepsilon_2/(\varepsilon_3\varepsilon_4)]}}. \quad \text{(D44)}$$

This is exact in both limits.

[1] P. M. Chaikin and T. C. Lubensky, *Principles of Condensed Matter Physics* (Cambridge University Press, Cambridge, UK, 2000).

[2] J. D. Gunton, M. San Miguel, and P. S. Sahni, in *Phase Transitions and Critical Phenomena*, edited by C. Domb and J. L. Lebowitz (Academic Press, New York, 1983), Vol. 8.

[3] J. A. N. Filipe and A. J. Bray, Phys. Rev. E **50**, 2523 (1994).

[4] A. J. Bray, Adv. Phys. **43**, 357 (1994).

[5] S. A. Safran, P. S. Sahni, and G. S. Grest, Phys. Rev. B **28**, 2693 (1983).

[6] P. S. Sahni, D. J. Srolovitz, G. S. Grest, M. P. Anderson, and S. A. Safran, Phys. Rev. B **28**, 2705 (1983).

[7] A. Polkovnikov, K. Sengupta, A. Silva, and M. Vengalattore, Rev. Mod. Phys. **83**, 863 (2011).

[8] E. Altman, Strongly Interacting Quantum Systems out of Equilibrium, in *Lecture Notes of the Les Houches Summer School* (Oxford University Press, Oxford, UK, 2016).

[9] C. Gogolin and J. Eisert, Nat. Phys. **11**, 124 (2015)

[10] J. Eisert, M. Friesdorf, and C. Gogolin, Rep. Prog. Phys. **79**, 056001 (2016).

[11] J. Li, W. Huang, B. Shteynas, S. Burchesky, F. Cagri Top, E. Su, J. Lee, A. O. Jamison, and W. Ketterle, Phys. Rev. Lett. **117**, 185301 (2016).
[12] J. Li, W. Huang, B. Shteynas, S. Burchesky, F. Cagri Top, E. Su, J. Lee, A. O. Jamison, and W. Ketterle, Nature **543**, 91 (2017).
[13] G. Wirth, M. Ölschläger, and A. Hemmerich, Nat. Phys. **7**, 147 (2011).
[14] M. Ölschläger, G. Wirth and A. Hemmerich, Phys. Rev. Lett. **106**, 015302 (2011).
[15] T. Kock, M. Ölschläger, A. Ewerbeck, W.-M. Huang, L. Mathey, and A. Hemmerich, Phys. Rev. Lett. **114**, 115301 (2015)
[16] L. W. Clark, L. Feng, and C. Chin, Science **354**, 606-610 (2016).
[17] L. Feng, L. W. Clark, A. Gaj, and C. Chin, Nature Phys. **14**, 269 (2018).
[18] B. M. Anderson, L. W. Clark, J. Crawford, A. Glatz, I. S. Aranson, P. Scherpelz, L. Feng, C. Chin, and K. Levin, Phys. Rev. Lett. **118**, 220401 (2017).
[19] C. V. Parker, L.-C. Ha, and C. Chin, Nat. Phys. **9**, 769 (2013).
[20] T. Müller, S. Fölling, A. Widera, and I. Bloch, Phys. Rev. Lett. **99**, 200405 (2007).
[21] W. V. Liu and C. Wu, Phys. Rev. A **74**, 013607 (2007).
[22] A. Isacsson and S. M. Girvin, Phys. Rev. A **72**, 053604 (2005).
[23] A. B. Kuklov, Phys. Rev. Lett. **97**, 110405 (2006).
[24] C. Xu and M. P. A. Fisher, Phys. Rev. B **75**, 104428 (2007).
[25] V. W. Scarola and S. Das Sarma, Phys. Rev. Lett. **95**, 033003 (2005)
[26] M. Ölschläger, T. Kock, G. Wirth, A. Ewerbeck, C. Morais Smith, and A. Hemmerich, New J. Phys. **15**, 083041 (2013).
[27] M. Di Liberto, A. Hemmerich, C. Morais Smith, Phys. Rev. Lett. **117**, 163001 (2016).
[28] X. Li, A. Paramekanti, A. Hemmerich, W. Vincent Liu, Nat. Commun. **5**, 3205 (2014).
[29] L. Niu, S. Jin, X. Chen, X. Li, and X. Zhou, Phys. Rev. Lett. **121**, 265301 (2018)
[30] H. Lignier, C. Sias, D. Ciampini, Y. Singh, A. Zenesini, O. Morsch, and E. Arimondo, Phys. Rev. Lett. **99**, 220403 (2007).
[31] M. A. Garcia-March *et al.*, New J. Phys. **20**, 113039 (2018).
[32] Leo P. Kadnoff and G. Baym, *Quantum Statistical Mechanics*, (W. A. Benjamin, New York, 1962).
[33] Yu. M. Kagan, B. V. Svistunov, and G. V. Shlyapnikov, J. Exp. Theor. Phys. **75**, 279 (1992)
[34] D. V. Semikoz and I. I. Tkachev, Phys. Rev. Lett. **74**, 3093 (1995)
[35] M. Holland, J. Williams, K. Coakley, and J. Cooper, Quant. Semiclass. Opt. **8**, 571 (1996)
[36] L. D. Landau and E. M. Lifshitz, *Statistical Physics*, 3rd ed. (Butterworth-Heinemann, Oxford, UK, 2013)
[37] S. Paul and E. Tiesinga, Phys. Rev. A **88**, 033615 (2013).
[38] K. Levin, A. Fetter, and D. Stamper-Kurn, *Ultracold Bosonic and Fermionic Gases* (Elsevier, Amsterdam, 2012).
[39] A. C. Newell, T. Passot, and J. Lega, Ann. Rev. Fluid Mech. **25**, 399 (1993).
[40] P. G. Kevrekidis and D. J. Frantzeskakis, Mod. Phys. Lett. B **18**, 173 (2004).
[41] Jason H. V. Nguyen, De Luo, and Randall G. Hulet, Science **356**, 422 (2017).